PAPER

Check for updates

Sustainable versatile chitin aerogels: facile synthesis, structural control and high-efficiency acoustic absorption†

Jun-Nan Wan,[a] Qing-Yuan Chen, [ID][a] Jian-Cheng Jiang,[a] Wei Guo,[a] Xiaoqing Zuo,[c] Chunlong Fei,[d] Shanshan Yao[b] and Ju-Qi Ruan [ID] *[ab]

Bio-based materials with excellent acoustic absorption properties are in great demand in architecture, interior, and human settlement applications for efficient noise control. In this study, crayfish shells, a form of kitchen waste, are utilized as the primary material to produce ultralight and multifunctional chitin aerogels, which effectively eliminate noise. Different replacement solvents and freezing rates were employed to regulate the porous structures of chitin aerogels, and their resulting acoustic absorption performance was investigated. Results demonstrate that employing deionized water as the replacement solvent and utilizing a common-freeze mode (frozen *via* refrigerator at −26 °C) can produce chitin aerogels with larger porosity (96.26%) and apertures, as well as thicker pore walls. This results in superior broadband acoustic absorption performance (with a maximum absorption coefficient reaching 0.99) and higher Young's modulus (28 kPa). Conversely, chitin aerogels solvent-exchanged with *tert*-butyl alcohol or subjected to quick-freeze mode (frozen *via* liquid nitrogen) exhibit smaller porosity (92.32% and 94.84%) and apertures, thereby possessing stronger diffuse reflection of visible light (average reflectance of 94.30% and 88.18%), and enhanced low-frequency (500 to 1600 Hz) acoustic absorption properties. Additionally, the acoustic absorption mechanism of fabricated chitin aerogels was predicted using a simple three-parameter analysis Johnson–Champoux–Allard–Lafarge (JCAL) model. This study presents a novel approach to developing multifunctional biomass materials with excellent acoustic absorption properties, which could have a wide range of potential applications.

1 Introduction

Chitin aerogel is a highly promising bio-based porous material with numerous advantages such as abundant sources, versatility, high biocompatibility, and antibacterial properties. It has been widely applied in various fields, including wound care,[1–3] food packaging,[4] separators,[5] catalysts,[6] pollutant adsorption,[7–9] thermal management,[10,11] and electromagnetic interference shielding.[11] Owing to its superior 3D interconnected porous networks, chitin aerogel can serve as an ideal sustainable sound-absorbing material to effectively eliminate noise. However, there have been few efforts devoted to studying the acoustic absorption behavior of chitin aerogels. The dissipation

of sound energy by a porous material, such as viscous and thermal losses, arises from the interaction of air molecules at the gas–solid interfaces within its interconnected pore channels.[12] Therefore, it is of significant importance to investigate the acoustic absorption properties of chitin aerogel by adjusting its porous structures.

Up to now, numerous studies have successfully manipulated the porous structures of chitin-based aerogels by adjusting the pore characteristics of their hydrogels through various methods, such as controlling the chitin matrix content[13–17] or incorporating additives,[18–22] regulating acid/alkali solvents,[23,24] employing neutralization processes,[25] ultrasonication,[5] *etc.*, followed by supercritical[2] or evaporation[26] drying techniques. But beyond those approaches, controlling the growth pattern of ice crystals during the freeze-casting process offers significant advantages in terms of robust controllability and high stability. Consequently, it demonstrates substantial potential for precisely adjusting the porous structures of chitin aerogels. Solvent exchange for chitin hydrogels is a critical method for effectively regulating the porous characteristics of chitin aerogels by controlling the size of ice crystal growth.[6,27] During freeze-casting, the fully filled solvents with varying volume expansibility may give rise to ice crystals of different sizes.

[a]*School of Physics Science and Technology, Kunming University, Kunming 650214, PR China. E-mail: ruanjuqi@foxmail.com*

[b]*School of Materials Science and Engineering, Jiangsu University, Zhenjiang 212013, PR China*

[c]*Faculty of Materials Science and Engineering, Kunming University of Science and Technology, Kunming 650093, PR China*

[d]*School of Microelectronics, Xidian University, Xi'an 710126, PR China*

† Electronic supplementary information (ESI) available. See DOI: https://doi.org/10.1039/d4ra03687e

Subsequently, the suspended chitin fibers will be compressed by these varied ice crystals, resulting in chitin aerogels with diverse porous characteristics once the ice crystals have sublimated. Liu et al.[28] investigated the influence of tert-butyl alcohol (TBA)/water binary solvents on the porous structures of chitin nanofibril aerogels via freeze-casting. The results indicate that: chitin nanofibril aerogels prepared from pure water solvent can exhibit micrometer-sized large pores and membrane-like walls. When the TBA concentration ranged from 10% to 50% in the binary solvents, the aerogels displayed relatively smaller pores with fibril-like networks. Furthermore, they developed micrometer-sized pores with thick layers when the TBA concentration reached 70%. Besides, freezing rate (controlled by the freezing temperature) is an equally critical factor to conveniently adjust the porous structures of chitin aerogels. Lower temperatures promote rapid nucleation and growth of ice crystals, resulting in a fine structure for chitin aerogels. Conversely, higher temperatures slow down the nucleation and growth rate of ice crystals, leading to sufficient crystal growth and the formation of macroporous structures.[29–32] For instance, Osada et al.[33] fabricated the β-chitin nanofiber aerogels (β-ChNF) by lyophilization at various freezing speeds. β-ChNF obtained by conventional freezing (-25 °C) exhibited an increased average aperture (43 μm) and reduced relative surface area ($\sim$8 m^2 g^{-1}) compared to those produced by rapid freezing with liquid nitrogen (7 μm, $\sim$27 m^2 g^{-1}). Furthermore, alternative methods for controlling the growth pattern of ice crystals, such as directional freezing[34–36] or freeze-thaw cycling,[25] have been reported to create anisotropic and hierarchical structures in chitin aerogels.

The aforementioned researches have powerfully demonstrated the excellent control of chitin aerogel's porous structures, endowing it with significant potential for efficient absorption of environmental noise. Apart from a few reports on the acoustic absorption behaviors of chitin-derived (i.e., chitosan) aerogels,[37–40] the acoustic absorption performance of chitin aerogels has not been studied yet. Here, the porous structures of the fabricated chitin aerogels were regulated by selecting alternative solvents or controlling the rate of freezing. We investigated the influence of structural control on the acoustic absorption properties of these chitin aerogels using experiments in combination with a simple three-parameter analysis model derived from the Johnson–Champoux–Allard–Lafarge (JCAL) theory. The results may provide a new perspective for conveniently fabricating multifunctional chitin aerogels tailored for acoustic absorption behaviors.

2 Experimental section

2.1 Materials

Crayfish shells were collected from kitchen wastes. Potassium hydroxide (KOH, ≥85%), Urea (≥99%), and tert-butyl alcohol (TBA, ≥99.5%) were provided by Xilong Scientific Co., Ltd. (Shantou, China). Sodium chlorite (NaClO$_2$, 80%) was purchased from Shanghai Macklin Biochemical Technology Co., Ltd. (Shanghai, China). Hydrochloric acid (HCl, 36–38%) was purchased from Chengdu Chron Chemical Co., Ltd.

(Chengdu, China). Ethanol (≥99.7%) was purchased from Rionlon Bohua (Tianjin) Pharmaceutical & Chemical Co., Ltd. (Tianjin, China). All chemical reagents are of analytical grade and used as received without further purification. Deionized water (DI water) is of laboratory grade and used throughout the experiments.

2.2 Extraction of purified chitin from crayfish shells

Crayfish shells were cleansed, dried, and ground into powders. Shell powders were first degreased in ethanol at 80 °C for 8 h, then they were immersed in 5 wt% NaClO$_2$ solution (pH = 3) for 5 h at 80 °C to remove the natural pigment. Next, depigmented powders were further demineralized via 6 wt% HCl solution at 80 °C for 3 h, followed by taking off the protein in 6 wt% KOH solution for 3 h at 90 °C. These treatments were repeated twice, and the product of each step was washed to neutral via DI water. Last, the product was filtered and dried to generate purified chitin powders in Fig. 1.

2.3 Fabrication of chitin aerogels

The preparation process of chitin aerogels in this study is shown schematically in Fig. 1. First, 1 g chitin powders were dissolved in 200 g KOH/urea/DI water hybrid solution (mass ratio of 11 : 4 : 85) to prefreeze at -26 °C for 12 h, and then thawed at room temperature combining with adequate stir to form a viscous and transparent chitin solution.[27] Later, plenty of ethanol was added to above chitin solution to generate the macroscopical chitin flocculation. After a while, the obtained chitin flocculation was subjected to adequate solvent-exchange by using TBA or DI water, respectively. Subsequently, the chitin flocculation was evenly dispersed in urea solution, afterwards centrifuged by a high-speed centrifuge (JIDI-16D, Guangzhou, China) for 3 min with the speed of 6000 rpm. After removing the supernatant, the residues were transferred to a set mold and densified to give chitin hydrogels. Finally, the hydrogels were frozen and then dried in a vacuum freeze-drying equipment (NAI-L4-80D, Shanghai, China) for 48 h, to fabricate chitin aerogels. Concretely, as shown in Fig. 1, chitin hydrogels replaced by solvent of DI water were subjected to a quick-freeze (frozen by liquid nitrogen) or common-freeze (frozen via the refrigerator at -26 °C) process, and the obtained chitin aerogel is named as Ln-DCA or R-DCA, respectively. The hydrogel replaced by solvent of TBA was frozen via the common-freeze process, and the prepared chitin aerogel is labeled as R-TCA.

2.4 Characterizations

Appearance of the specimens was analyzed through optical photographs. The cross-sectional morphology of chitin aerogels was observed using a scanning electron microscopy (SEM, Hitachi S-3400 N, Tokyo, Japan) at a relatively low accelerating voltage of 3 kV. The specimens were sputter-coated with platinum before the test to achieve clear imaging as a result of an increased conductivity of the sample surface. Mercury intrusion porosimetry (MIP) test was conducted via a mercury porosimetry analyzer (Micromeritics AutoPore IV 9510, Atlanta, GA, USA) to quantitatively analysis the pore structure characteristics of
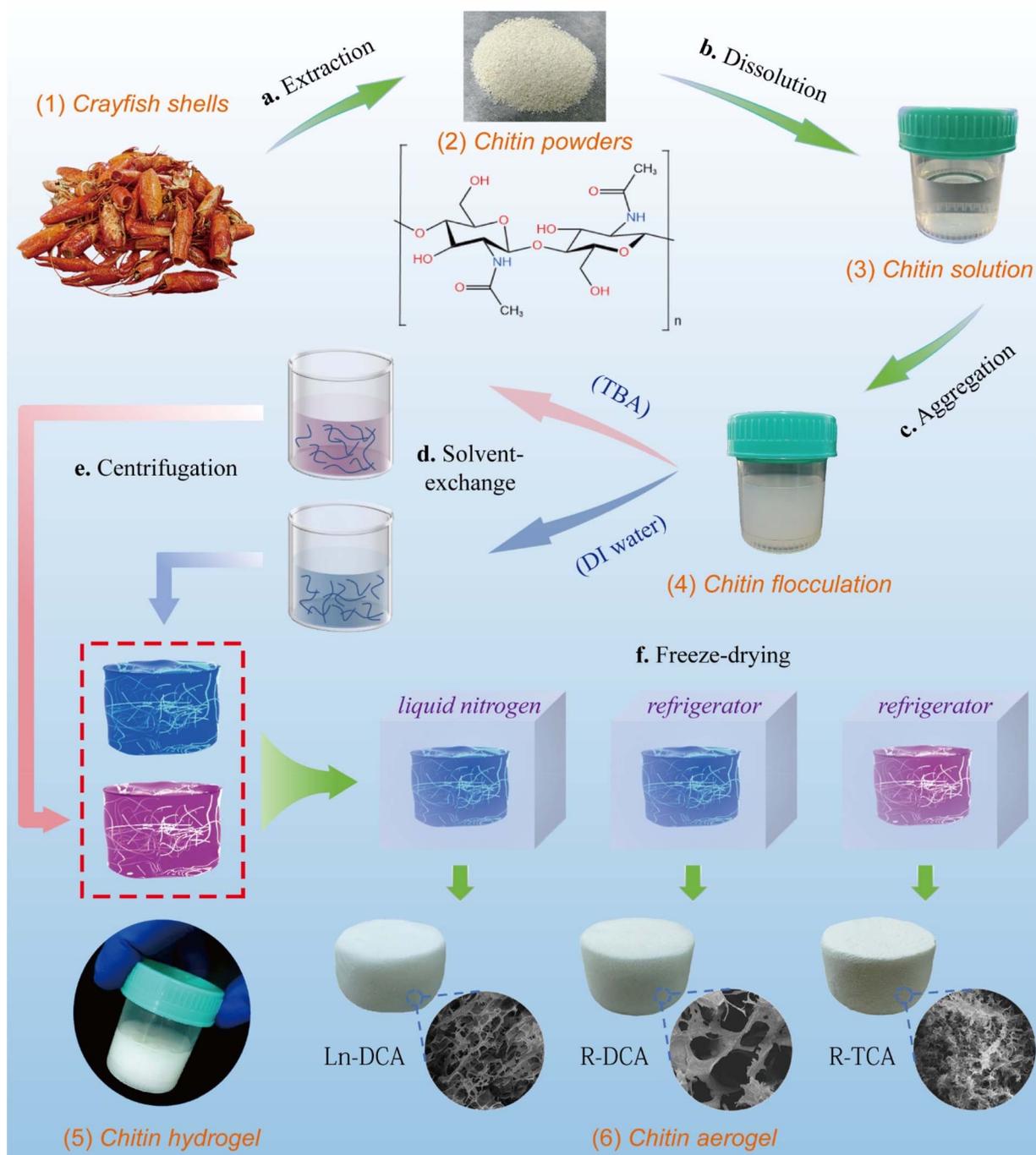
Fig. 1 Schematic illustration for the fabrication pathway of sustainable and multifunctional chitin aerogels.

chitin aerogels, *e.g.*, aperture distribution pattern, porosity, bulk density, and feature apertures (average, median, or most probable aperture), covering a recognizable aperture range of 5 nm to 800 μm. Fourier Transform Infrared (FT-IR) measurements were carried out on a FT-IR spectrometer (Bruker Tensor 27, Saarbrucken, Germany) to validate the chemical structures of specimens in a wavenumber range from 400 to 4000 cm^{-1} with a resolution of 0.96 cm^{-1}. The thermal stability of chitin aerogels was assessed through thermogravimetric (TG) and derivative thermogravimetry (DTG) results obtained *via* a thermogravimetry (Netzsch TG 209 F1, Selb, Germany), and the specimens were heated from room temperature to 800 °C at a heating rate of 10 °C min^{-1} in nitrogen atmosphere. The normal incident acoustic absorption coefficient was employed to evaluate the acoustic absorption performance of chitin aerogels, and was tested using a BSWA SW477 impedance tube (Beijing, China) based on a two-microphone transfer function method according to the ISO 10534-2:2023 standard.[41] The measurement range of acoustic absorption frequency is 500–6300 Hz. Mechanical performance (*e.g.*, Young's modulus) was

evaluated through a uniaxial quasi-static compression test according to the GB/T 1041-2008 standard.[42] Chitin aerogels were loaded into a universal testing machine (MTS CMT6103, Eden Prairie, MN, USA) at an invariant cross-head speed of 1 mm min^{-1}. Chitin aerogels used for acoustical and mechanical testing were processed in cylinders with height of 15 mm and diameter of 30 mm. A spectrophotometer (Shimadzu UV-3600i Plus, Kyoto, Japan) was adopted to test the diffuse reflectance of chitin aerogels crossing visible light wavelengths from 390 to 800 nm.

3 Results and discussion

3.1 Regulation of the porous structure of chitin aerogels

Fig. 2a–c depicts the optical photographs of R-TCA, Ln-DCA, and R-DCA, respectively. They can each be smoothly placed on the flower's pistils due to their ultralow bulk density, as shown in Fig. 2d. During lyophilization, the sublimation of ice crystals prevents liquid capillary pressure from damaging porous structures,[43] resulting in fabricated chitin aerogels with a complete appearance devoid of cracks and shrinkage. In general, all these chitin aerogels possess cellular morphology regardless of the replacement solvent's type and freezing speed. The cross-section SEM images of R-TCA (Fig. 2a′) and R-DCA (Fig. 2c′) reflect that adopting DI water as the replacement solvent during solvent-exchange process facilitates the formation of larger micron-sized pores in chitin aerogels compared to those replaced by TBA solvent. Following freezing, low-temperature vacuum drying sublimates the ice crystals, creating pores of corresponding size that are direct replicas of the frozen solvent. Hence, R-DCA obtains larger pores since the higher volume expansibility of DI water during freezing may cause adequate growth of ice crystals. This phenomenon can also be quantitatively confirmed by referring to Fig. 2e and Table 1. Compared with R-TCA, the aperture distribution of R-DCA concentrates in a relatively larger aperture range from 80
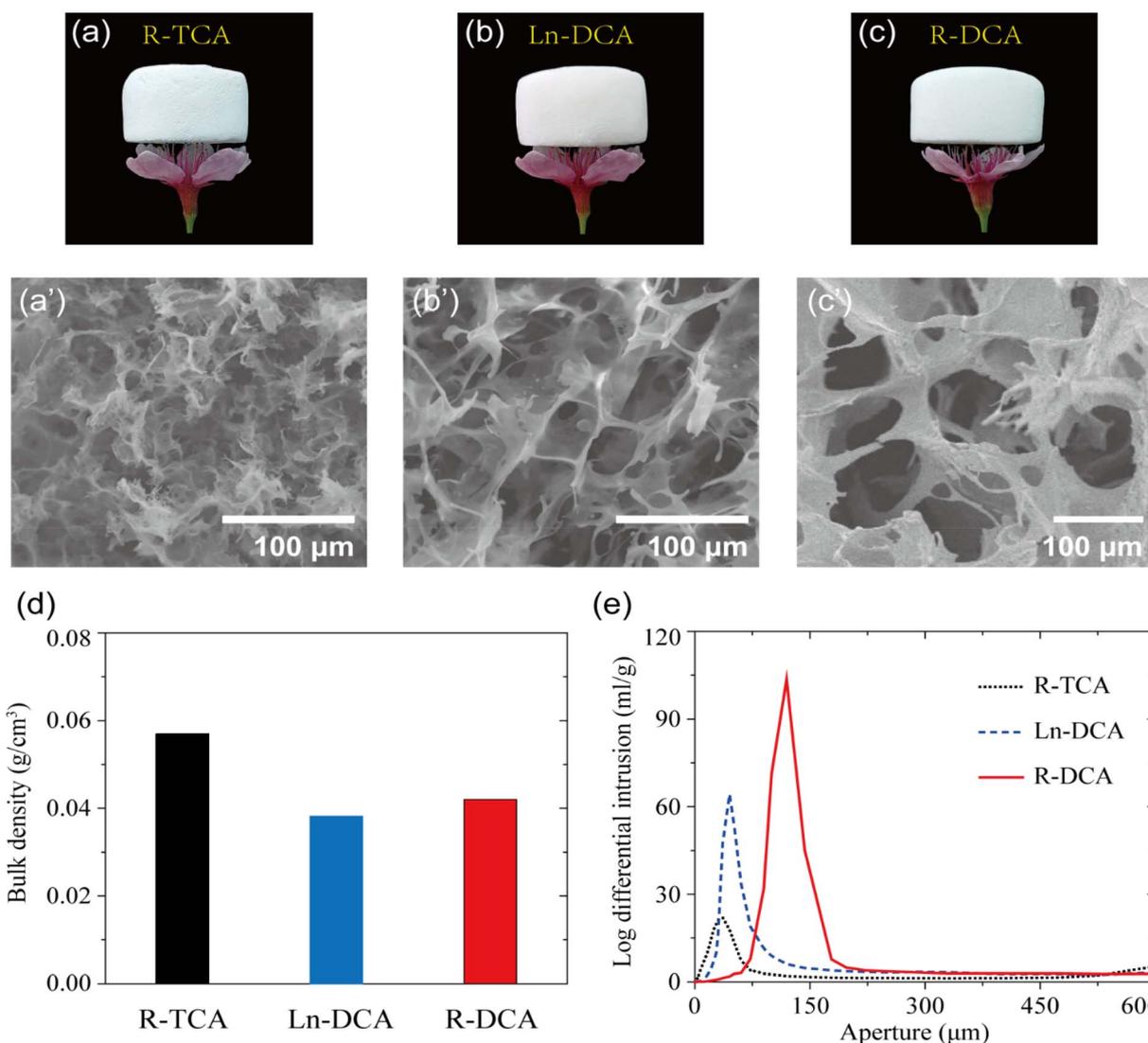

Fig. 2 (a–c) Optical photographs of fabricated chitin aerogels sitting on the flower. (a′–c′) SEM images of chitin aerogels. (d) Bulk density of chitin aerogels. (e) Aperture distribution pattern of chitin aerogels.

Table 1 Porous structural features of fabricated chitin aerogels

	Porosity (%)	Average aperture (μm)	Median aperture (μm)	Most probable aperture (μm)
R-TCA	92.32	8.22	30.75	36.23
Ln-DCA	94.84	47.74	48.57	45.24
R-DCA	96.26	108.27	115.63	119.50

to 180 μm. At the same time, R-DCA possesses obviously higher feature apertures (average, median, and most probable aperture, Table 1) and porosity (96.26%, Table 1, higher than the chitosan/urea aerogel reported in ref. 26), and exhibits a lower bulk density (0.042 g cm^{-3}, Fig. 2d) compared to R-TCA. Besides using solvent-exchange, the porous structures of fabricated chitin aerogels are purposefully regulated through different freezing rates. It can be clearly seen that compared to R-DCA, Ln-DCA exhibits smaller pores and thinner walls (Fig. 2b′ and c′) with a lower aperture distribution range located from 30 to 70 μm (Fig. 2e), and meanwhile possesses a decreased porosity (94.84%, Table 1), feature apertures, and bulk density (0.038 g cm^{-3}, Fig. 2d, lower than the chitin aerogels reported in ref. 24 and 27). This can be briefly interpreted as the rapid freezing process by liquid nitrogen facilitates extremely fast nucleation and growth rates, resulting in the formation of tiny ice crystals and, consequently, a fine structure for chitin aerogels after sublimation. In summary, we effectively regulated the porous structure of chitin aerogels through the use of different replacement solvents or freezing rates, thereby imparting them with distinct physical and chemical properties for practical applications.

3.2 Chemical structure of chitin aerogels

FT-IR test was employed to determine the main functional groups present in the structure of fabricated chitin aerogels, and the main results are summarized in Table 2. As shown in Fig. 3, the FT-IR spectra of chitin aerogels is quite similar to that of purified chitin. The vibration peaks at 1313 cm^{-1} and 1260 cm^{-1} are corresponded to C–C–O stretching of chitin's glycosidic ring, and bands at 1157 cm^{-1}, 1071 cm^{-1}, 1027 cm^{-1} (the position of the dotted lines in Fig. 3) correspond to the typical O–C–C stretching of the glycosidic ring.[44] The two peaks at 3266 cm^{-1} and 3106 cm^{-1} are caused by the stretching

Table 2 Observed FT-IR absorption wavenumbers and assignment of the spectrum of fabricated chitin aerogels

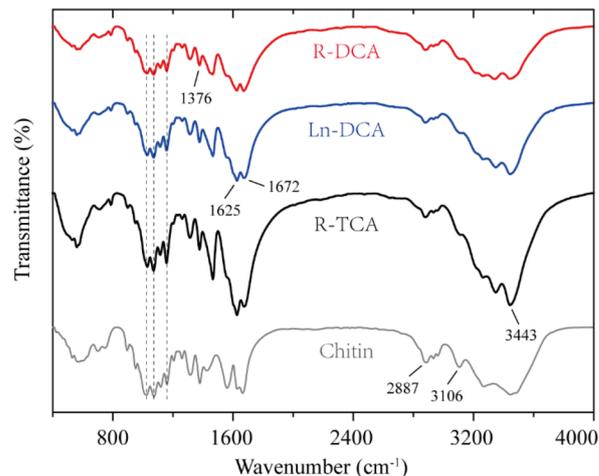| Assignment	Peak positions (cm^{-1})
C–C–O stretch vibration	1313, 1260
O–C–C stretch vibration	1157, 1071, 1027
N–H stretch vibration	3266, 3106
NH$_2$ out-of-plain bending vibration	897
Asymmetric C–H stretch vibration	2960, 2933
Symmetric C–H stretch vibration	2887
C=O stretch vibration	1672, 1625
C–N stretch vibration	1376
O–H stretch vibration	3443

Fig. 3 FT-IR vibrational spectra of purified chitin and chitin aerogels.

vibration of N–H bond, and the peak at 897 cm^{-1} is due to the out-of-plain bend of the NH$_2$ group.[45] The bands at 2960 cm^{-1} and 2933 cm^{-1} are asymmetric C–H stretching, and the one at 2887 cm^{-1} is due to symmetric C–H stretch.[44] The vibrational bands located at 1672 cm^{-1} and 1625 cm^{-1} are due to the C=O stretch of the amide group contained in the chitin structure.[1,2,46] Besides, the absorption peak at 1376 cm^{-1} is assigned to the C–N stretch, and the band centered in 3443 cm^{-1} is the stretching of the alcohols' O–H bond presented in the chitin structure.[44] These are the typical characteristic peaks of chitin molecules, which indicate that the purified chitin was successfully extracted from crayfish shells. Importantly, the FT-IR results strongly prove that the adopted dispersion/aggregation process in Fig. 1 did not change the main structural components of chitin, which is conducive to rapidly preparing high-purity chitin aerogels.

3.3 Thermal stability of chitin aerogels

In view of the significance of thermal stability in practical applications, the thermal decomposition behaviors of as-prepared chitin aerogels were investigated through thermogravimetric analysis under nitrogen atmosphere. As shown in Fig. 4a, the TG curves of chitin aerogels showed similar trends with four main pyrolysis stages: (1) initial pyrolysis (below 100 °C), (2) stability at low temperatures (100 to 150 °C), (3) severe pyrolysis (150 to 400 °C), and (4) stability at high temperatures (above 400 °C). In stage (1), the slight weight losses around 3–5% apparently resulted from evaporation of adsorbed water.[27] Since the relatively low temperatures in stage (2) are insufficient to cause the decomposition of chitin molecules, the weight losses of specimens are mainly assigned to the further evaporation of residual adsorbed water, hence resulting in the flat TG curves. The chitin aerogels underwent intense pyrolysis in stage (3) including the chemical degradation of urea (150 to 230 °C), urea's pyrolysis products (230 to 320 °C), and the chitin component (320 to 400 °C).[23] As shown in Fig. 4b, the obvious pyrolysis peak of DTG curves located at the temperature ranges of 186.8 to 188 °C, 289 to 296.7 °C, and 356 to 362.6 °C,
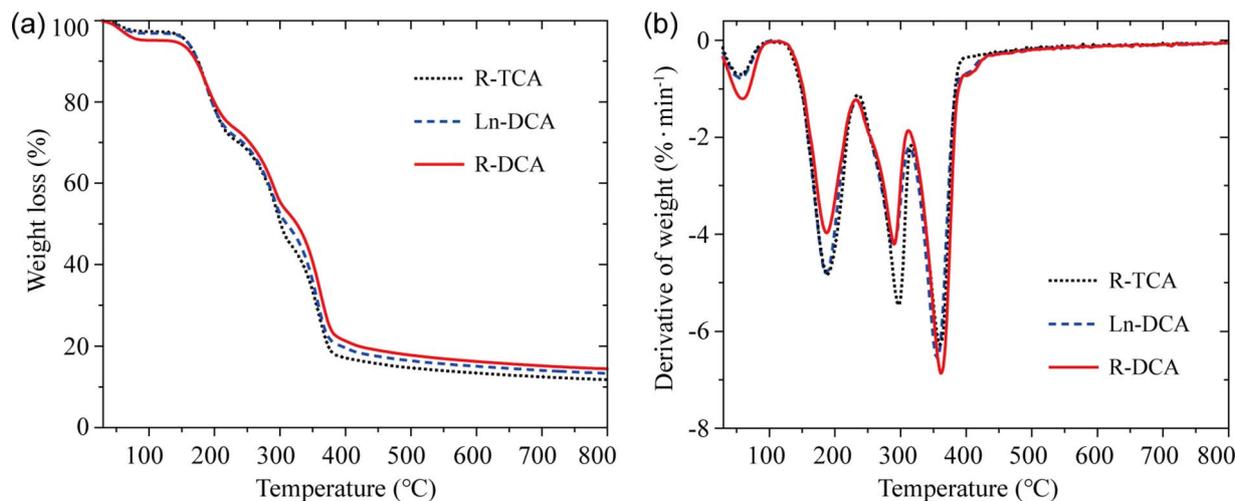
Fig. 4 TG (a) and DTG (b) curves of chitin aerogels under nitrogen atmosphere.

corresponds to the typical decomposition for urea, urea by-products, and the chitin, respectively. When the temperature continues rising to stage (4), the strong-bound water contained in the chitin aerogel is almost lost, causing the TG curves to flatten gradually. TG and DTG results validate good heat resistance (working temperature up to 200 °C) for fabricated chitin aerogels, which is sufficient to meet the demand for thermal stability in human settlement applications.

3.4 Acoustic absorption performance of chitin aerogels

Acoustic absorption performance reflected by absorption coefficient was investigated to evaluate the noise reduction ability of fabricated chitin aerogels. Fig. 5a shows the normal incident acoustic absorption coefficient (A) of chitin aerogels within 500 to 6300 Hz. Table 3 summarizes their acoustic absorption properties including the peak and average absorption coefficient (A_p, A_{ave}), and bandwidth (BW). Inside, BW is defined as
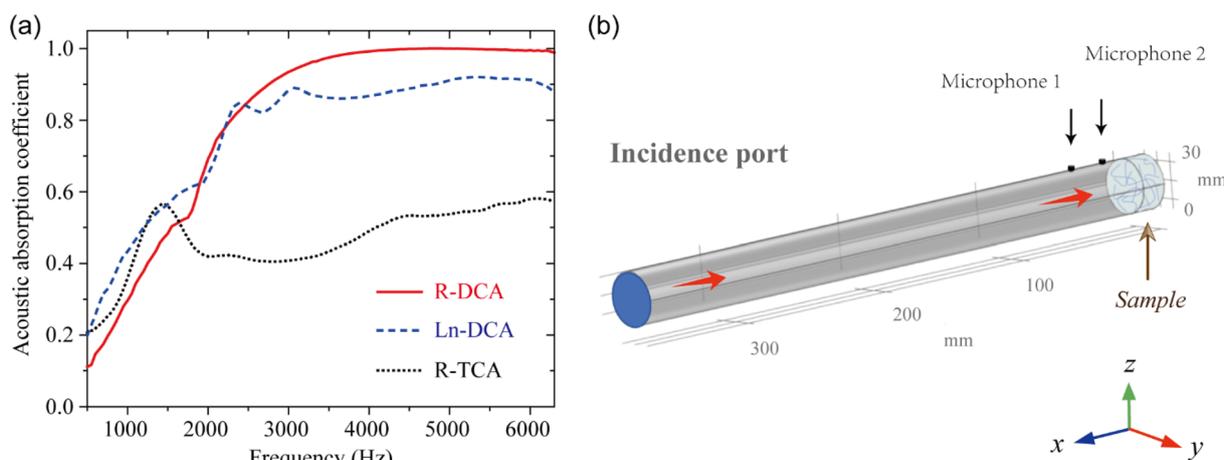

Fig. 5 (a) Acoustic absorption performance of chitin aerogels. (b) Schematic diagram of the three-parameter JCAL model to simulate acoustic absorption behaviors of chitin aerogels.

Table 3 Acoustical, mechanical, and optical properties of fabricated chitin aerogels

	R-TCA	Ln-DCA	R-DCA
Peak absorption coefficient A_p	0.58 (6100 Hz)	0.92 (5350 Hz)	0.99 (4850 Hz)
Average absorption coefficient A_{ave}	0.47	0.77	0.80
Bandwidth BW ($A > 0.9$) (Hz)	0	1250	3500
Young's modulus (kPa)	26	18	28
Diffuse reflectance (to visible light) (%)	94.30	88.18	82.37

the width of the frequency band with absorption coefficient above 0.9. The characteristics of chitin aerogels' porous structure significantly influence their acoustic absorption behaviors. Typically, R-DCA exhibits superior acoustic absorption property than R-TCA (Fig. 5a) with extremely higher values of A_p, A_{ave}, and BW (Table 3). Meanwhile, the BW of R-DCA is obviously higher than the chitin-derived aerogels reported in literature.[37–40] Excellent absorption performance of R-DCA can be explained *via* its porous structural features. In one aspect, compared to R-TCA, R-DCA is able to achieve higher acoustic impedance matching at the incident surface owing to its lower density (0.042 g cm^{-3}, Fig. 2d).[47] Combining with the larger characteristic apertures (Table 1), when wide-band airborne sound incidents on the surface of R-DCA, the vibrating air molecules (*e.g.*, N_2 and O_2) can easily enter the material's interior with less obstruction.[48] In another aspect, the higher porosity (96.26%, Table 1) makes R-DCA own larger gas–solid interfacial area within its pore channels. Sound energy will be efficiently dissipated at these considerable gas–solid interfaces in forms of viscous or thermal losses,[49] hence resulting in extremely high acoustic absorption. In addition, it can be found that R-TCA possesses higher absorption capacity than R-DCA in the low frequency domain (below 1600 Hz). This can be interpreted as the lower porosity of R-TCA (92.32%, Table 1) may cause higher obstacles for acoustic waves to propagate in the material's interior, and then prolong their propagation paths. The extended path length of acoustic waves in R-TCA will lead to a higher possibility of energy dissipation with a longer quarter-wavelength condition, therefore enhancing absorption abilities at lower frequencies.[50] By the same mechanism, the different acoustic absorption properties of R-DCA and Ln-DCA can also be mainly explained as the porous features of Ln-DCA (*e.g.*, the lower porosity of 94.84%, Table 1) leads to poor acoustic absorption due to weaker viscous/thermal losses, however provides a longer sound propagation path length to effectively dissipate low-frequency (below 1600 Hz) acoustic waves. In

order to verify the acoustic absorption mechanism of fabricated chitin aerogels, we used COMSOL Multiphysics to develop numerical simulation of their porous structures combining finite element method *via* a simple three-parameter analysis JCAL model.[51] As shown in Fig. 5b, chitin aerogel (clings to a rigid back) was equivalent to a homogeneous medium represented by its three structural parameters: porosity, characteristic aperture, and standard deviation of the characteristic aperture. The surface acoustic impedance of such homogeneous medium can be predicted *via* the three structural parameters to further calculate the acoustic absorption coefficient. Here, based on the aperture distribution characteristics of fabricated chitin aerogels (Fig. 2e), the most probable aperture (Table 1) was chosen to simulate the acoustic absorption coefficient. The results show that (Fig. S1–S3 of the ESI†), to a certain degree, the employed three-parameter model can predict the acoustic absorption behavior of as-prepared chitin aerogels, and indicates their noise reduction mechanisms.

3.5 Multifunctional properties of chitin aerogels

Apart from acoustic absorption performance, the mechanical and optical properties of prepared chitin aerogels were investigated to verify their versatility. The mechanical property was evaluated by the axial quasi-static compression test. Fig. 6a shows the stress–strain curves of chitin aerogels at 80% strain. The compressive performance of chitin aerogels is closely dependent on their porous structures. Since the deformation in elastic region (strain below 0.5%, Fig. 6a) is mainly caused by the slight twisting of aerogels' pore wall,[52] R-DCA with thicker pore walls (Fig. 2a′–c′) owns stronger anti-deformation ability and possesses a higher Young's modulus of 28 kPa (Table 3). The plastic deformation of chitin aerogels, however, are vitally interrelated with their bulk densities. As shown in Fig. 6a, chitin aerogels with larger bulk densities (*e.g.*, R-TCA) are favorable to withstand greater external compression. This can be simply
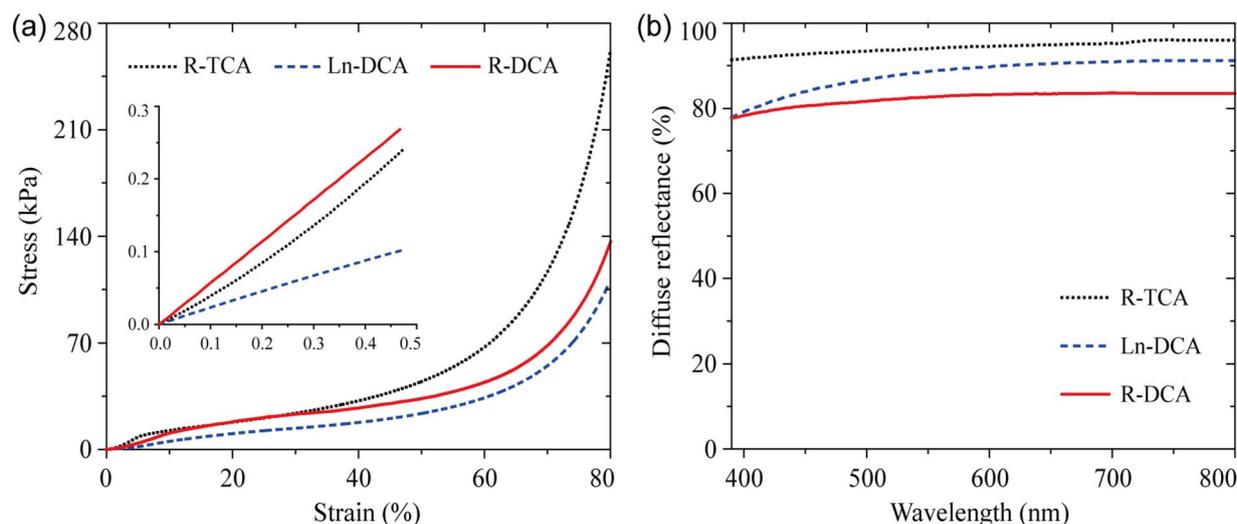

Fig. 6 (a) Compression stress–strain curves of chitin aerogels. Insert shows the typical elastic deformation region. (b) Diffuse reflectance of chitin aerogels within the visible light region.

explained as the higher density may provide a denser porous structure for chitin aerogel to better resist the considerable plastic collapse and bending of its pore walls. With the compressive strain increasing (above 60%), the chitin aerogels are densified and thus show strong strain hardening while without obvious disruption, exhibiting superior flexibility and deformability for potential applications.[5]

Fig. 6b shows the optical property of chitin aerogels represented by the diffuse reflectance within the visible light band. All the chitin aerogels exhibit excellent broadband reflection characteristics owing to the dense nano-scattering centers enriched on their surfaces,[53] and hence give them the white appearance (Fig. 2a–c). And it is noteworthy that the porous structure still determines the diffuse reflectance of chitin aerogels. Clearly, their diffuse reflectance increases with the decrease of characteristic apertures as well as the porosity (Table 1). This is mainly because the smaller aperture and porosity may effectively prevent light waves from entering the material, and then result superior diffuse reflection performance due to the irregular pore morphology. Notably, the average diffuse reflectance of R-TCA can be as high as 94.30%, showing its unique advantage for indoor light management.

4   Conclusions

We successfully prepared the multifunctional lightweight chitin aerogels using a simple dispersion/aggregation process followed with freeze-drying. The porous structures of chitin aerogels were regulated by altering the replacement solvent type or freezing rate. The results indicate that using DI water as the replacement solvent or employing a lower freezing speed leads to the production of chitin aerogels with larger characteristic apertures, higher porosity, and thicker pore walls. Consequently, these aerogels exhibit superior broadband acoustic absorption performance and a higher Young's modulus. However, the chitin aerogel solvent-exchanged with *tert*-butyl alcohol or obtained by quick-freeze mode possesses smaller porosity and apertures, hence exhibiting higher diffuse reflection to visible light, and the increased low-frequency noise reduction ability. This study not only paves the way for the recycling of biomass wastes, but also provides a new perspective to develop sustainable and efficient sound-absorbing materials with big application potential in various fields including construction, vehicle, and environmental acoustics.

Data availability

The raw/processed data required to reproduce these findings cannot be shared at this time as the data also form part of an ongoing study.

Author contributions

JQR: conceptualization, funding acquisition, methodology, writing – original draft and writing – review & editing. JNW: investigation, methodology, software and writing – original draft. QYC and JCJ: validation. WG and XZ: resources and funding acquisition. CF: software. SY: project administration and supervision.

Conflicts of interest

The authors declare that they have no conflict of interest.

Acknowledgements

References

1 K. Kang, Y. Liu, X. Song, L. Xu, W. Zhang, Y. Jiao and Y. Zhao, *Macromol. Biosci.*, 2022, **22**, 2200020.

2 X. Guo, D. Xu, Y. Zhao, H. Gao, X. Shi, J. Cai, H. Deng, Y. Chen and Y. Du, *ACS Appl. Mater. Interfaces*, 2019, **11**, 34766–34776.

3 L. E. Nita, A. Ghilan, A. G. Rusu, I. Neamtu and A. P. Chiriac, *Pharmaceutics*, 2020, **12**, 449.

4 H. Haghighi, F. Licciardello, P. Fava, H. W. Siesler and A. Pulvirenti, *Food Packag. Shelf Life*, 2020, **26**, 100551.

5 X. Yang, X. Zhang, D. Li, Y. Zhou, X. Ren, Q. Zhang, T. Jiang, D. Shi and J. You, *J. Power Sources*, 2023, **580**, 233398.

6 Y. Tsutsumi, H. Koga, Z.-D. Qi, T. Saito and A. Isogai, *Biomacromolecules*, 2014, **15**, 4314–4319.

7 W. Ye, J. Xi, Y. Sun, L. Meng, H. Bian, H. Xiao and W. Wu, *Int. J. Biol. Macromol.*, 2023, **249**, 125958.

8 J. Kuang, T. Cai, J. Dai, L. Yao, F. Liu, Y. Liu, J. Shu, J. Fan and H. Peng, *Int. J. Biol. Macromol.*, 2023, **230**, 123238.

9 J. Xu, Y. Zhang, J. He, J. Wu, W. Li, H. Zhang, H. Wang, J. Tu, Y. Zhou, Y. Dong and D. Zhu, *ACS Sustainable Chem. Eng.*, 2021, **9**, 5000–5009.

10 Y. Yan, F. Ge, Y. Qin, M. Ruan, Z. Guo, C. He and Z. Wang, *Carbohydr. Polym.*, 2020, **248**, 116755.

11 X. Zhang, K. Qian, J. Fang, S. Thaiboonrod, M. Miao and X. Feng, *Nano Res.*, 2023, **17**, 2038–2049.

12 T. Budtova, T. Lokki, S. Malakooti, A. Rege, H. Lu, B. Milow, J. Vapaavuori and S. L. Vivod, *Adv. Eng. Mater.*, 2022, **25**, 2201137.

13 L. Heath, L. Zhu and W. Thielemans, *ChemSusChem*, 2013, **6**, 537–544.

14 I. V. Tyshkunova, D. G. Chukhchin, I. V. Gofman, E. N. Pavlova, V. A. Ushakov, E. N. Vlasova, D. N. Poshina and Y. A. Skorik, *Materials*, 2021, **14**, 5191.

15 Y. Huang, J. Yang, L. Chen and L. Zhang, *ACS Sustainable Chem. Eng.*, 2018, **6**, 10552–10561.

16 K. Gao, Y. Guo, Q. Niu, H. Fang, L. Zhang, Y. Zhang, L. Wang and L. Zhou, *Cellulose*, 2018, **25**, 4591–4602.

17 M. He, Z. Wang, Y. Cao, Y. Zhao, B. Duan, Y. Chen, M. Xu and L. Zhang, *Biomacromolecules*, 2014, **15**, 3358–3365.

18 J. Wang, Z. Chen and H. E. Naguib, *Carbohydr. Polym.*, 2021, **265**, 118014.

19 I. Shahzadi, Y. Wu, H. Lin, J. Huang, Z. Zhao, C. Chen, X. Shi and H. Deng, *J. Hazard. Mater.*, 2023, **453**, 131312.

20 L. Liu, L. Bai, A. Tripathi, J. Yu, Z. Wang, M. Borghei, Y. Fan and O. J. Rojas, *ACS Nano*, 2019, **13**, 2927–2935.

21 R. Gao, Y. Lu, S. Xiao and J. Li, *Sci. Rep.*, 2017, **7**, 4303.

22 L. Liu, X. Li, R. Zhou and Y. Fan, *Carbohydr. Polym.*, 2024, **324**, 121523.

23 R. Wang, L. Liu, J. Yu, Z. Wang, L. Hu and Y. Fan, *Cellulose*, 2017, **24**, 5443–5454.

24 B. Ding, D. Zhao, J. Song, H. Gao, D. Xu, M. Xu, X. Cao, L. Zhang and J. Cai, *Sci. China: Chem.*, 2016, **59**, 1405–1414.

25 P. Ratanajiajaroen, M. Ohshima and J. Supercrit, *Fluid*, 2012, **68**, 31–38.

26 N. Guerrero-Alburquerque, S. Zhao, N. Adilien, M. M. Koebel, M. Lattuada and W. J. Malfait, *ACS Appl. Mater. Interfaces*, 2020, **12**, 22037–22049.

27 B. Ding, J. Cai, J. Huang, L. Zhang, Y. Chen, X. Shi, Y. Du and S. Kuga, *J. Mater. Chem.*, 2012, **22**, 5801–5809.

28 H. Chen, L. Liu, F. Chen, Y. Fan and Q. Yong, *Carbohydr. Polym.*, 2022, **283**, 119138.

29 X. Qian, P. Ren, X. Liu, Y. Du, H. Li, X. Shi and F. Ding, *Mater. Lett.*, 2018, **228**, 229–231.

30 X. Chen, M. Zhou, Y. Zhao, W. Gu, Y. Wu, S. Tang and G. Ji, *Green Chem.*, 2022, **24**, 5280–5290.

31 H. Zhang, C. Liu, L. Chen and B. Dai, *Chem. Eng. Sci.*, 2019, **201**, 50–57.

32 Y. Tian, D. Estevez, H. Wei, M. Peng, L. Zhou, P. Xu, C. Wu, M. Yan, H. Wang, H.-X. Peng and F. Qin, *Chem. Eng. J.*, 2021, **421**, 129781.

33 S. Suenaga and M. Osada, *Int. J. Biol. Macromol.*, 2019, **126**, 1145–1149.

34 Y. Zhou, S. Fu, Y. Pu, S. Pan and A. J. Ragauskas, *Carbohydr. Polym.*, 2014, **112**, 277–283.

35 J. Shan, D. Liu, F. Su, M. Li, H. Tian, M. Guo, W. Qiao, J. He, Q. Li and J. Qian, *ACS Sustainable Chem. Eng.*, 2020, **8**, 17387–17396.

36 X. Li, L. Zhu, T. Kasuga, M. Nogi and H. Koga, *Chem. Eng. J.*, 2022, **450**, 137943.

37 T.-T. Li, K. Zang, X. Wang, C.-W. Lou and J.-H. Lin, *ACS Appl. Nano Mater.*, 2023, **6**, 20149–20160.

38 X. Jiang, J. Zhang, F. You, C. Yao, H. Yang, R. Chen and P. Yu, *Appl. Clay Sci.*, 2022, **228**, 106624.

39 S. Takeshita, S. Akasaka and S. Yoda, *Mater. Lett.*, 2019, **254**, 258–261.

40 K. Zang, X. Wang, L. Liu, H.-k. Peng, H.-T. Ren, L. Zhang, J.-H. Lin, C.-W. Lou and T.-T. Li, *Cellulose*, 2024, **31**, 3573–3588.

41 ISO10534-2, *Standard Terminology for Acoustics – Determination of Acoustic Properties in Impedance Tubes - Part 2: Two-Microphone Technique for Normal Sound Absorption Coefficient and Normal Surface Impedance*, Geneva, Switzerland, 2023.

42 *GB/T 1041-2008 Standard Terminology for Plastics – Determination of Compressive Properties*, Beijing, China, 2008.

43 B. T. Mekonnen, W. Ding, H. Liu, S. Guo, X. Pang, Z. Ding and M. H. Seid, *J. Leather Sci. Eng.*, 2021, **3**, 25.

44 S. P. Druzian, N. P. Zanatta, R. K. Borchardt, L. N. Côrtes, A. F. M. Streit, E. C. Severo, J. O. Gonçalves, E. L. Foletto, E. C. Lima and G. L. Dotto, *Int. J. Biol. Macromol.*, 2021, **179**, 366–376.

45 S. Kumar and S. B. Rai, *Indian J. Pure Appl. Phys.*, 2010, **48**, 251–255.

46 J. Moreno-Pérez, P. S. Pauletto, A. M. Cunha, Á. Bonilla-Petriciolet, N. P. G. Salau and G. L. Dotto, *Colloids Surf., A*, 2021, **614**, 126170.

47 T. Han, X. Wang, Y. Xiong, J. Li, S. Guo and G. Chen, *Composites, Part A*, 2015, **78**, 27–34.

48 M. A. Kuczmarski and J. C. Johnston, *Acoustic Absorption in Porous Materials, NASA/TM-2011-216995*, National Aeronautics and Space Administration, Clevend, OH, USA, 2011.

49 J.-S. Kim, M. Mahato, J. H. Oh and I. K. Oh, *Adv. Mater. Interfaces*, 2022, **10**, 2202092.

50 H. Choe, G. Sung and J. H. Kim, *Compos. Sci. Technol.*, 2018, **156**, 19–27.

51 K. V. Horoshenkov, A. Hurrell and J.-P. Groby, *J. Acoust. Soc. Am.*, 2019, **145**, 2512–2517.

52 G. Kumar, D. T. K. Dora, A. Jadav, A. Naudiyal, A. Singh and T. Roy, *J. Cleaner Prod.*, 2021, **298**, 126744.

53 L. Hu, G. Zheng, J. Yao, N. Liu, B. Weil, M. Eskilsson, E. Karabulut, Z. Ruan, S. Fan, J. T. Bloking, M. D. McGehee, L. Wågberg and Y. Cui, *Energy Environ. Sci.*, 2013, **6**, 513–518.